



In-depth study of spectroscopic properties of new Pr^{3+} -ion doped low-phonon sesquisulfide Lu_2S_3 material for mid-IR laser sources

Martin Fibrich ^{a,c,*}, Jan Šulc ^a, Lubomír Havlák ^b, Vítězslav Jaryš ^b, Robert Král ^b, Vojtěch Vaněček ^b, David Vyhlička ^a, Helena Jelínková ^a, Martin Nikl ^b

^a Faculty of Nuclear Sciences and Physical Engineering, Czech Technical University in Prague, Břehová 7, Prague 1 115 19, Czech Republic

^b Institute of Physics of the Czech Academy of Science, Cukrovarnická 10, Prague 6 162 00, Czech Republic

^c The Extreme Light Infrastructure ERIC, ELI Beamlines Facility, Za Radnicí 835, Dolní Břežany 252 41, Czech Republic



ARTICLE INFO

Keywords:

Binary sulfides
Sesquisulfides
Low-phonon laser materials
Rare-earth doping
Mid-infrared lasers

ABSTRACT

Lu_2S_3 material from the family of sesquisulfide hosts appears to be a promising low-phonon material for use as a laser gain medium allowing for a laser emission over a broad spectral range from ultraviolet to far mid-infrared wavelengths. In this paper, a praseodymium-ion doped Lu_2S_3 single crystal grown by micro-pulling down technique is investigated with focus on its spectroscopic properties. The Raman, excitation, and luminescence spectra are presented. By selective excitation of the main energy levels of Pr^{3+} -ions, 26 luminescence transitions of the $\text{Pr:Lu}_2\text{S}_3$ crystal spanning the $\sim 0.49 - 5.5 \mu\text{m}$ wavelength range have been identified. The correct assignment of the observed luminescence spectra to the respective Pr^{3+} energy-level transitions was confirmed by the calculation of the optimized squared reduced-matrix elements for the tensor operators $\mathbf{U}^{(k)}$ and $\mathbf{L} + g\mathbf{S}$.

1. Introduction

The search for low-phonon laser materials doped with rare-earth (RE) ions is of particular interest for the development of mid-infrared (mid-IR) laser sources. Mid-IR solid-state lasers are attractive due to their wide range of potential applications, including remote sensing, molecular spectroscopy, atmospheric sensing, optical metrology, medicine, etc. Compared to optical parametric oscillators (OPOs) which are commonly used to cover this spectral range, solid-state lasers based on the direct generation of the mid-IR radiation offer greater sturdiness and simplicity.

To achieve laser emission in the mid-IR spectral region, it is crucial to select a host material with a low phonon energy. Lower phonon energies reduce the probability of multi-phonon relaxation processes of excited states. This leads to lower non-radiative losses and higher fluorescence quantum yields [1,2]. The maximum phonon energies determine the minimum number of phonons required for multi-phonon transitions between two energy levels with a given energy gap. A general guideline suggests that the laser transition energy should exceed five times the maximum phonon energy to avoid multiphonon-assisted relaxation [3].

Following this guideline, one can deduce that a laser host with a maximum phonon energy of $E_{ph} \leq 300 \text{ cm}^{-1}$ is necessary for achieving an acceptable quantum efficiency for the longest ever reported laser transition of $\sim 7 \mu\text{m}$ (1500 cm^{-1}) [4].

Efficient pulsed laser operation at the longest reported wavelength of $7.2 \mu\text{m}$ has been demonstrated in Pr^{3+} -ion doped LaCl_3 [4]. This material has a maximum phonon energy of only 210 cm^{-1} . However, the main drawback of such simple tri-chloride crystals, like LaCl_3 , ErCl_3 , YCl_3 , etc., is that these materials suffer poor mechanical properties and requires special handling and storage due to its strong hygroscopicity [5, 6]. More practical low-phonon laser materials are RE-ion doped alkali-lead halides with general formula of MPb_2X_5 ($\text{M} = \text{Rb}, \text{K}; \text{X} = \text{Cl}, \text{Br}$), having the lowest phonon energies ($E_{ph} \sim 140 - 200 \text{ cm}^{-1}$) ever reported in crystalline laser matrices [1-3,7,8]. These crystals are low- or non-hygroscopic, have satisfactory mechanical properties, and are able to incorporate RE ions fairly easily, although the high concentrations are difficult to achieve [1,9]. Laser emission was successfully demonstrated with KPb_2Cl_5 doped by Pr^{3+} , Nd^{3+} , Dy^{3+} , or Er^{3+} ions [10-13,14]. Suitable and well-developed low-phonon host materials for mid-IR laser generation are also chalcogenide crystals like Cr^{2+} and Fe^{2+}

* Corresponding author at: Faculty of Nuclear Sciences and Physical Engineering, Czech Technical University in Prague, Břehová 7, Prague 1 115 19, Czech Republic.

E-mail addresses: martin.fibrich@fjfi.cvut.cz (M. Fibrich), jan.sulc@fjfi.cvut.cz (J. Šulc), havlak@fzu.cz (L. Havlák), jary@fzu.cz (V. Jaryš), kral@fzu.cz (R. Král), vaneciek@fzu.cz (V. Vaněček), david.vyhlidal@fjfi.cvut.cz (D. Vyhlička), helena.jelinkova@fjfi.cvut.cz (H. Jelínková), nikl@fzu.cz (M. Nikl).

doped II-VI semiconductor compounds [15–18–21] with typical representatives of ZnSe or ZnS ($E_{ph} \sim 200 - 350 \text{ cm}^{-1}$) or thiogallates CaGa₂S₄ or PbGa₂S₄, for which laser action was obtained under Dy³⁺ doping [10,22–24]. The great advantage of these materials is their low or zero hygroscopicity. However, they usually have low acceptance of RE-dopants, which limits the doping concentration to a few tenths of a percent [3]. New promising moisture-resistant low-phonon ($E_{ph} \sim 220 \text{ cm}^{-1}$) chalcogenide materials, tolerant to the concentration of dopants from the lanthanide group are the ternary alkali RE sulfides with general formula ALnS₂ (A = K, Rb; Ln = La, Gd, Lu), represented e.g. by KLuS₂ material [25–28]. However, the preparation of this material is challenging, and current methods can only synthesize crystals in the form of 40 μm thick hexagonal plates [28]. This fact restricts the practical use of this material as an active medium for mid-IR laser sources.

Another interesting family of low-phonon laser hosts is the family of binary sulfides, also known as sesquisulfides for the composition RE₂S₃ where RE is the rare-earth element and S is sulfur. The sesquisulfides of the trivalent RE are a large family of high bandgap semiconductors with potential applications as optical IR window materials, thermoelectric and magneto-optical materials, photocatalysts, and laser phosphors, etc. [29–32,33]. These materials have several unique properties such as a high refractive index (2 – 2.8), a broad transparency range (0.5 – 20 μm), and a wide region of homogeneity of physical properties [29, 34].

This contribution focuses on the Lu₂S₃ crystal, which has been successfully grown in bulk form. The material is highly stable and exhibits chemical resistivity comparable to that of ZnSe [35]. However, unlike II-VI semiconductor compounds, its structure makes it highly suitable for lanthanide doping. Thus, the RE-doped sesquisulfides have the potential to be an interesting alternative to the well-developed ZnS and ZnSe materials, with the aim of extending the range of available laser wavelengths in the mid-IR region. This article describes the spectroscopic properties of Pr³⁺ ion-doped Lu₂S₃ crystals, successively grown by micro-pulling-down method [36]. The main focus is on excitation and luminescence spectra which are firstly (to our best knowledge) described up to 5.4 μm . Raman spectroscopy is also presented, confirming the low-phonon energy of the Lu₂S₃ matrix, comparable to the well-established solid-state active media in the mid-IR wavelength region, such as ZnS, ZnSe, PbGa₂S₄ etc.

It should be noted that Pr³⁺-ions are well-established RE dopants for solid state laser hosts operating mainly in the wide spectral range in the visible region [37], but the Pr³⁺ energy level structure allows for a possible laser transitions in the near- and mid-IR spectral regions. Therefore, the knowledge of the luminescence spectra up to far mid-IR is justified. The simplified energy level diagram of Pr³⁺-ion along with the

observed luminescence transitions of the Pr:Lu₂S₃ is displayed in Fig. 1.

2. Material and methods

2.1. Sample preparation

Pr:Lu₂S₃ crystals were grown from melt using a modified micro-pulling-down method under an inert argon atmosphere in a graphite crucible and multilayer alumina shielding. Such arrangement was necessary due to high melting temperature of Lu₂S₃ reaching $\sim 1750^\circ\text{C}$. After melting the material and seeding, the Lu₂S₃ crystals were pulled with growth rate around 0.1 mm/min. In this way, Pr:Lu₂S₃ crystals with Pr³⁺-ion concentration of 0.05 at. % Pr/Lu and 0.5 at. % in melt Pr/Lu were prepared. Due to the small size (area) of the samples and relatively low Pr³⁺ concentrations in the melt, accurate measurement of Pr³⁺ content in the sample proved to be challenging. However, X-ray fluorescence analysis of the Pr(0.5 at. %):Lu₂S₃ sample estimated the Pr³⁺ concentration to be around 0.3 at. % Pr/Lu, closely matching the nominal melt composition. For Pr(0.05 at. %):Lu₂S₃, it was not possible to measure it. Therefore, hereafter we will refer to the concentration in the melt. It is worth mentioning, the distribution of Pr³⁺ will be influenced by segregation in both axial and radial directions. However, given the growth conditions used for the micro-pulling-down growth of Lu₂S₃, segregation is expected to be significantly reduced compared to crystals grown using the Czochralski technique [38,39]. Accurate determination of the effective segregation coefficient of Pr³⁺ in Lu₂S₃, both axially and radially, will be addressed in future studies.

It should be also noted that due to the unavailability of high-quality Lu₂S₃ single crystals to serve as seeds, a graphite rod was utilized instead. This approach is standard practice during the initial growth stages of novel materials. Subsequently, the Lu₂S₃ crystal obtained from the graphite seed can itself be employed as a seed crystal for further growth cycles. Detail description of Pr:Lu₂S₃ crystals growth is shown in [36].

Samples for spectroscopic characterization were prepared by cutting and polishing the grown bulk material into $\sim 1.5 \text{ mm}$ in diameter and $\sim 1 \text{ mm}$ in length pieces.

A photograph of the Pr:Lu₂S₃ sample (0.05 at. % of Pr³⁺) is shown in Fig. 2. The sample is transparent, however, it contains black inclusions in some parts. These inclusions are most likely graphite that is released from the hot zone elements during the growth process. To avoid this phenomenon, the use of crucible made from alternative materials must be considered. However, selecting an appropriate crucible for the growth of high-temperature sulfides presents significant challenges. High-melting-point metals such as molybdenum, tungsten, or even

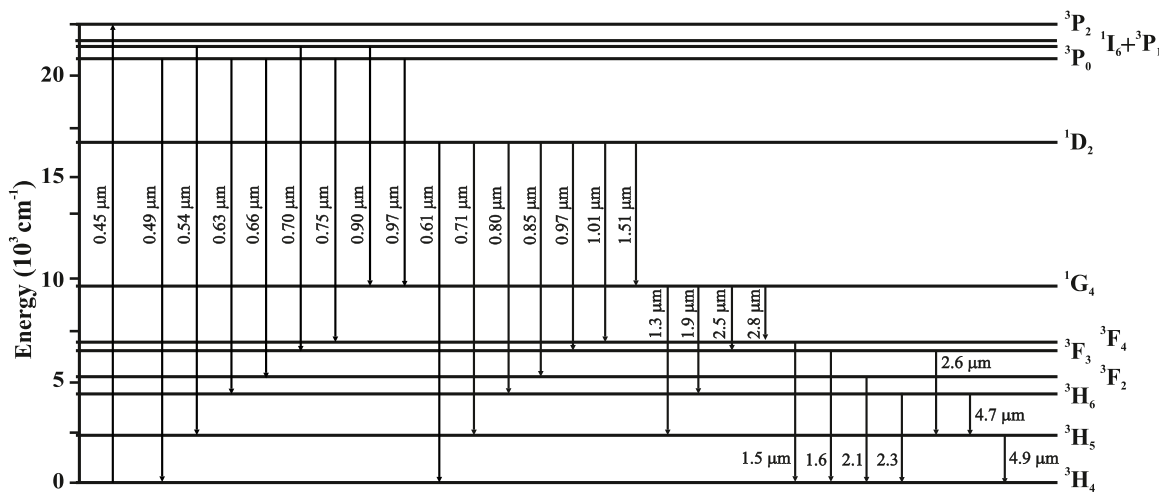


Fig. 1. Simplified energy level structure of Pr³⁺ ions with indication of observed and identified Pr³⁺ luminescence transitions in Lu₂S₃ laser host.

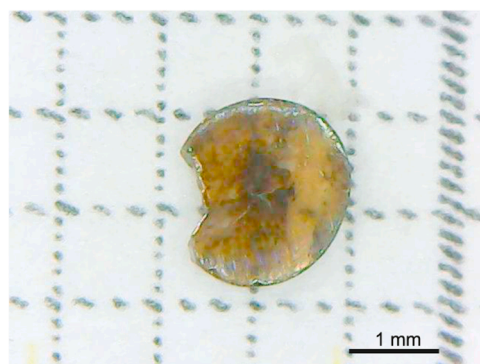


Fig. 2. Photograph of Pr:Lu₂S₃ sample (0.05 at. % of Pr³⁺).

iridium are not chemically inert toward sulfide melts at elevated temperatures. While graphite exhibits chemical resistance to sulfide melts, it tends to release particulate at high temperatures. To mitigate this issue and enhance crystal quality, we plan to utilize crucibles made from glassy carbon. However, fabricating custom-made glassy carbon crucibles of such small dimensions involves specialized manufacturing processes, making their production both time-consuming and costly.

In addition, based on our experience with the micro-pulling-down growth of oxide materials, we anticipate the formation of sulfur vacancies in the crystals when these are grown under an inert atmosphere. This issue could be mitigated by employing an argon-hydrogen sulfide gas mixture as the growth atmosphere. However, due to the toxicity of hydrogen sulfide, strict safety precautions must be implemented. Additionally, other defects, such as oxygen substitution at sulfur sites, may also occur in the resulting crystals.

2.2. Methods of characterization

The Raman spectrum of the Pr:Lu₂S₃ (0.05 at. % of Pr³⁺) sample was measured using a Raman spectrometer Wasatch Photonics WP830 (Raman spectral range 100 – 1800 cm⁻¹, resolution 6 cm⁻¹).

The absorption spectra of the sample are typically measured directly using a spectrophotometer. However, direct measurement was hindered by the presence of black inclusions in our samples (see Fig. 2), which could potentially lead to distorted results. Therefore, to identify the absorption maxima of the Pr:Lu₂S₃, the excitation spectra measurement was performed. The investigated sample was excited by a tunable laser Ekspla NT252-1k-SH and the corresponding intensities of the fluorescence spectra were recorded as a function of the excitation wavelengths using appropriate detectors (Thorlabs Si-detector FDS10X10, PbS-detector PDA30G-EC, or PbSe-detector PDA20H-EC) in combination with suitable band-pass or long-pass filters.

The sample was then excited to its specific absorption maxima and the luminescence spectra were measured using the StellarNet BlueWave NIR-50 fiber coupled spectrometer (in the range of 490 – 1100 nm), StellarNet DwarfStar fiber coupled spectrometer (970 – 1700 nm), and stepper-motor-driven monochromator ORIEL 77250 (1900 – 5600 nm). The monochromator was equipped with a 77301 grating assembly (Newport, 150 grooves per mm) and micrometer-adjustable slits. To record the transmitted radiation intensity, the above mentioned PbS or PbSe detectors were used along with the appropriate long-pass filters to block signals from undesired diffraction orders.

3. Results and discussion

3.1. Raman spectra

The Raman spectrum of the Pr(0.05 at. %):Lu₂S₃ single crystal in the energy range of 100 – 550 cm⁻¹ is depicted in Fig. 3. The peak with a maximum at 157 cm⁻¹ probably corresponds to low-frequency

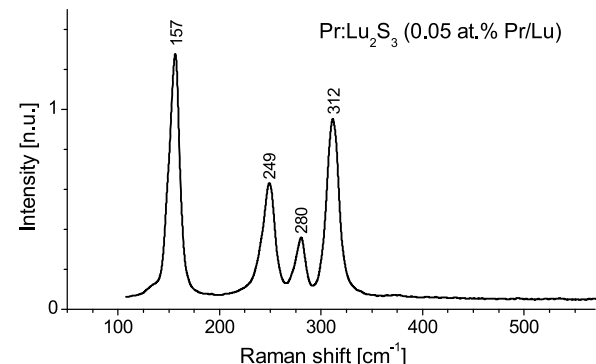


Fig. 3. Raman spectrum of Pr:Lu₂S₃ (0.05 at. % of Pr³⁺) crystal.

translational modes of Lu and S in the Lu₂S₃ lattice (deformation vibrations). The peak at 249 cm⁻¹ can then be related to the bending of the Lu-S bonds. The peak at 280 cm⁻¹ is probably the symmetric stretching mode A_g, while the peak at 312 cm⁻¹ can be identified as the antisymmetric stretching mode E_g. The highest observed energy peak position can be considered as a first approximation for the effective phonon energy of the crystalline matrices [8]. Therefore, in the case of Pr:Lu₂S₃, the maximum value of the phonon energy can be estimated to be $E_{ph} \sim 312$ cm⁻¹, which is a value comparable to other low-phonon laser hosts like ZnSe ($E_{ph} \sim 250$ cm⁻¹), ZnS ($E_{ph} \sim 350$ cm⁻¹), or PbGa₂S₄ ($E_{ph} \sim 350$ cm⁻¹).

3.2. Excitation spectra

Due to the nature of the samples, it was not possible to directly measure absorption spectra of the crystal to set the optimal wavelengths for particular energy-level excitations, as was mentioned in 2.2. For that reason, to determine the position of the absorption maxima for individual Pr³⁺-ion transitions, the excitation spectra were measured. The excitation spectra of the Pr:Lu₂S₃ crystal (0.05 at. % of Pr³⁺) are presented in Fig. 4 for the spectral range of 440 – 515 nm (Fig. 4a) and 590 – 635 nm (Fig. 4b). Sharp absorption lines typical for the Pr³⁺-ion can be identified in the distinctive laser transitions of $^3H_4 \rightarrow ^3P_{0,1,2}$ and $^3H_4 \rightarrow ^1D_2$, respectively. The main absorption maxima correspond to wavelengths of 456, 498, and 595 nm.

In the case of excitation spectra measurement in the infrared spectral range, a sample with a higher doping of active ions (0.5 at. % of Pr³⁺) was used. This was done to increase the absorption of the excitation radiation in the crystal, resulting in a stronger signal compared to the lower doped sample. The recorded excitation spectra related to infrared absorption are shown in Fig. 5. The obtained spectra in the ranges of 960–1110 nm, 1380 – 1750 nm, and 1900 – 2230 nm correspond to $^3H_4 \rightarrow ^1G_4$ (Fig. 5a), $^3H_4 \rightarrow ^3F_{3,4}$ (Fig. 5b), and $^3H_4 \rightarrow ^3F_2$ (Fig. 5c) transitions, respectively. The main absorption maxima, suitable for the further fluorescence excitation, correspond to wavelengths of 1022, 1556, 1638, and 2057 nm. The excitation spectrum for the $^3H_4 \rightarrow ^3H_6$ transition was not measured due to the low output energy of the excitation laser for the wavelengths above 2.3 μ m.

3.3. Pr:Lu₂S₃ wavefunctions optimization

Optimization of the 4f wavefunctions of rare-earth doped materials is essential to determine the relevant values of the reduced matrix elements of the $U^{(k)}$ ($k = 2, 4, 6$). This tensor characterizes the electric-dipole induced 4f-4f transition intensities. Tabulated values of $|\langle U^{(k)} \rangle|^2$, often based on aqueous RE³⁺ solutions, can differ from the optimized values for a specific matrix by up to tens of percent [40]. This discrepancy is subsequently transferred directly to the determination of the Judd-Ofelt intensity parameters. Therefore, without finding the

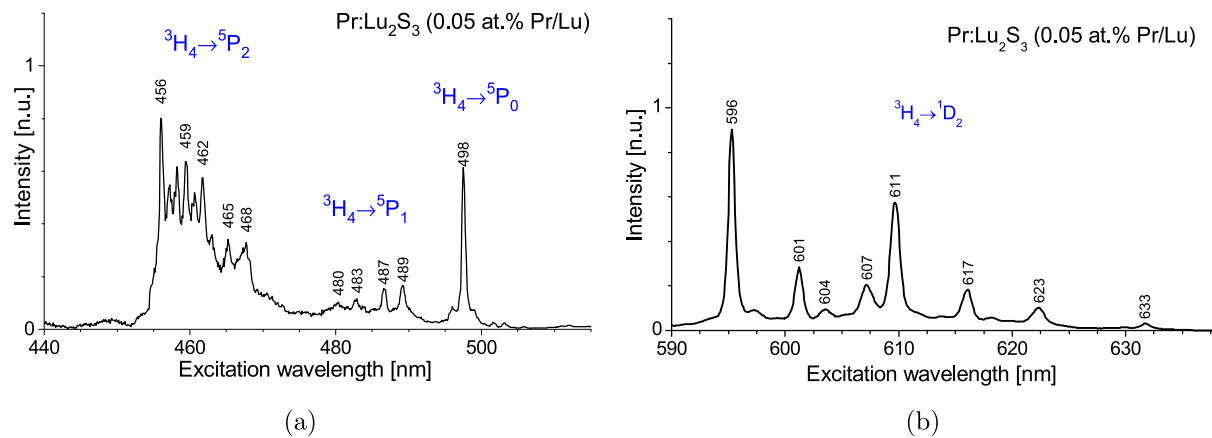


Fig. 4. Excitation spectra of 0.05% Pr:Lu₂S₃ for the spectral range of 440 – 530 nm (a), and 590 – 635 nm (b).

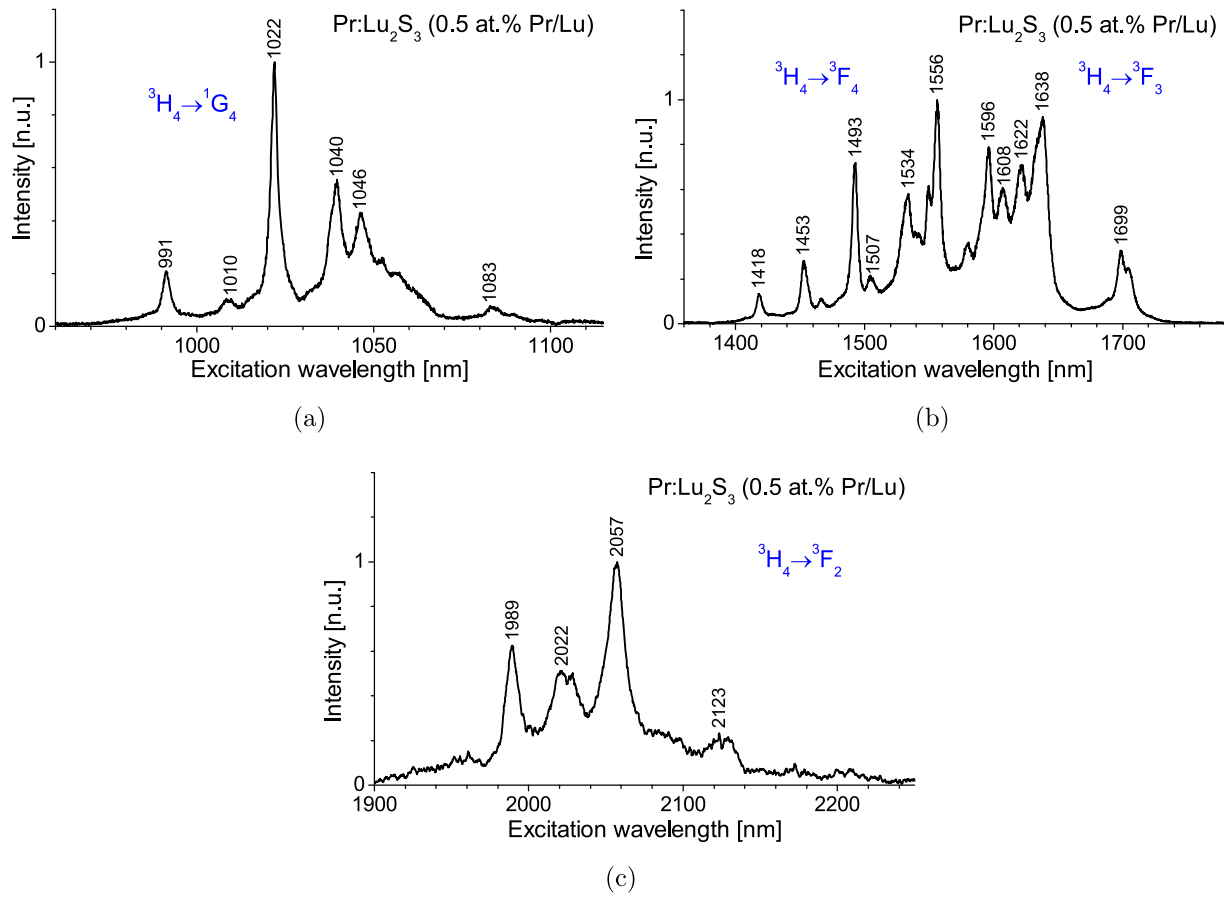


Fig. 5. Excitation spectra of 0.5% Pr:Lu₂S₃ for the spectral range of 960 – 1115 nm (a), 1380 – 1780 nm (b), and 1900 – 2280 nm (c).

optimized 4f wavefunction or $|\langle \mathbf{U}^{(k)} \rangle|^2$, it is not possible to accurately calculate the intensities of absorption and emission transitions.

To optimize the 4f wavefunctions of the investigated Pr:Lu₂S₃, the energies of the $^{2S+1}L_J$ multiplets must be known. These energies can be firstly determined as the barycenters of the respective transitions using the measured excitation spectra. The barycenter energy is then set as the weighted average energy for the specific transition, meaning that the integrated portions of the spectrum below and above this energy are equal. The determined barycenter energy values, along with the integration intervals, are listed in the Table 1. It should be noted that the determined barycenter values for the $^3H_4 \rightarrow ^3F_{3,4}$ transitions may be

subject to error due to the potential overlap of the bands and the uncertainty associated with the margin between the bands. It should be noted that although low-temperature excitation spectra measurements could help refine the determination of some $^{2S+1}L_J$ sublevel positions, a complete crystal-field analysis would be required to accurately determine the barycenter energies, which is laborious and not trivial task. Additionally, the improvement in the accuracy of 4f wave function optimization achieved through a detailed crystal-field analysis, compared to calculations based on room-temperature spectra measurement, is relatively small. For example, as demonstrated by Hehlen et al. [40] for Er:LaCl₃, using precise $^{2S+1}L_J$ multiplet energies (rather than values derived from room-temperature absorption spectra

Table 1

Input data for Pr:Lu₂S₃ wavefunctions optimization: integration intervals for barycenter determination; experimental barycenters obtained from the measured excitation spectra; barycenters calculated from optimized Hamiltonian matrix; calculated complete set of intermediate coupling wavefunctions.

Pr ³⁺ level	Integration range [cm ⁻¹]	Barycenter exp. [cm ⁻¹]	Barycenter calc. [cm ⁻¹]	Intermediate coupling wavefunction
³ H ₄			0	– 0.985 ³ H ₄ ⟩ – 0.168 ¹ G ₄ ⟩
³ H ₅	–	–	2077	+ 1.000 ³ H ₅ ⟩
³ H ₆	–	–	4242	– 0.998 ³ H ₆ ⟩ + 0.057 ¹ I ₆ ⟩
³ F ₂	4400 – 5300	4888	4687	– 0.988 ³ F ₂ ⟩ – 0.151 ¹ D ₂ ⟩
³ F ₃	5800 – 6365	6162	6073	+ 1.000 ³ F ₃ ⟩
³ F ₄	6365 – 7100	6494	6529	+ 0.804 ³ F ₄ ⟩ – 0.581 ¹ G ₄ ⟩ + 0.124 ³ H ₄ ⟩
¹ G ₄	8500 – 11,000	9639	9450	+ 0.796 ¹ G ₄ ⟩ + 0.593 ³ F ₄ ⟩ – 0.117 ³ H ₄ ⟩
¹ D ₂	15,000 – 17,200	16,479	16,450	– 0.944 ¹ D ₂ ⟩ + 0.295 ³ P ₂ ⟩ + 0.149 ³ F ₂ ⟩
³ P ₀	19,800 – 20,280	20,099	20,112	– 0.996 ³ P ₀ ⟩ – 0.094 ¹ S ₀ ⟩
¹ I ₆	–	–	20,124	+ 0.998 ¹ I ₆ ⟩ + 0.057 ³ H ₆ ⟩
³ P ₁	20,280 – 21,000	20,584	20,724	+ 1.000 ³ P ₁ ⟩
³ P ₂	21,100 – 22,150	21,727	21,945	+ 0.955 ³ P ₂ ⟩ + 0.294 ¹ D ₂ ⟩
¹ S ₀	–	–	47,360	– 0.996 ¹ S ₀ ⟩ + 0.094 ³ P ₀ ⟩

measurement) reduces the relative error in the barycenter determination, with an average energy deviation of about 40 cm⁻¹. Even for the lowest energy levels, this corresponds to a relative error of less than 0.5 %. Therefore, we believe that our approach, based on room-temperature data, still provides a significant improvement over calculations relying on absorption spectra measurements of aqueous RE³⁺ solutions.

The set of experimental barycenter energies was used to optimize wavefunctions for the Pr³⁺-doped Lu₂S₃. The procedure described in detail by Hehlen *et al.* [40] and the RELIC 1.0 software package documentation [41] was followed. Fitting the barycenter energies calculated from the optimized Hamiltonian matrix to a set of experimentally determined Pr³⁺ barycenters, electrostatic interaction parameters $F_{(2)} = (296.0 \pm 2.4)$ cm⁻¹, $F_{(4)} = (46.0 \pm 1.2)$ cm⁻¹, $F_{(6)} = (4.66 \pm 0.17)$ cm⁻¹, and spin-orbit interaction parameter $\zeta = (739 \pm 13)$ cm⁻¹ can be obtained. Using these material-specific parameters optimized for Pr:Lu₂S₃, we calculated the position of the barycenters for all Pr³⁺ levels and a complete set of intermediate coupling wavefunctions to see the impact of spin-orbit interaction (see Tab. 1).

It should be noted, the obtained interaction parameters $F_{(2, 4, 6)}$ and ζ for Pr:Lu₂S₃ are not significantly different from the average values of a large number of rare earth doped compounds (for Pr³⁺: $F_{(2)} = 306$ cm⁻¹, $F_{(4)} = 46.8$ cm⁻¹, $F_{(6)} = 4.57$ cm⁻¹, $\zeta = 746$ cm⁻¹ [40,41]) and one can expect that tensor operators $U^{(k)}$ and $L + gS$ for Pr:Lu₂S₃ will exhibit minimal discrepancy from the data available in the literature (e.g. [42]). This is basically true, but we have found that for some transitions (e.g. ³F₄ ↔ ³H₄, ¹G₄ ↔ ³H₄, ¹D₂ ↔ ³H₄, ³F₄ ↔ ³H₅, ³F₄ ↔ ³H₆, ¹G₄ ↔ ³H₆, ¹G₄ ↔ ³H₅, and ¹D₂ ↔ ³F₄), notable discrepancies of the order of tens percent can be observed. For that reason, we also present (for all Pr³⁺ transitions) the squared reduced-matrix elements for the tensor operators $U^{(k)}$ and $L + gS$, calculated with the help of $F_{(2, 4, 6)}$ and ζ interaction parameters optimized for Pr:Lu₂S₃ (see Table 2). These results were used to help identify transitions associated to some spectral lines in the measured Pr:Lu₂S₃ luminescence spectra. Furthermore, the results may be employed in a Judd-Ofelt analysis in the future once the Pr:Lu₂S₃ absorption cross-section data is available.

Table 2

Calculated set of optimized squared reduced-matrix elements for tensor operators $U^{(k)}$ and $L + gS$.

Transition	λ [μm]	$ \langle U^{(2)} \rangle ^2$	$ \langle U^{(4)} \rangle ^2$	$ \langle U^{(6)} \rangle ^2$	$ \langle L + gS \rangle ^2$
³ H ₅ ↔ ³ H ₄	4.81	0.1096	0.2007	0.6123	10.486
³ H ₆ ↔ ³ H ₅	4.62	0.1080	0.2327	0.6418	10.798
³ H ₆ ↔ ³ H ₄	2.36	0.0001	0.0338	0.1390	0
³ F ₂ ↔ ³ H ₆	22.5	0	0.0164	0.3044	0
³ F ₂ ↔ ³ H ₅	3.83	0	0.2979	0.6594	0
³ F ₂ ↔ ³ H ₄	2.13	0.5090	0.4032	0.1173	0
³ F ₃ ↔ ³ F ₂	7.22	0.0210	0.0510	0	6.513
³ F ₃ ↔ ³ H ₆	5.46	0	0.3181	0.8457	0
³ F ₃ ↔ ³ H ₅	2.50	0.6286	0.3468	0	0
³ F ₃ ↔ ³ H ₄	1.65	0.0653	0.3461	0.6980	0.007
³ F ₄ ↔ ³ F ₃	21.9	0.0255	0.0737	0.0053	4.367
³ F ₄ ↔ ³ F ₂	5.43	0.0012	0.0012	0.0907	0
³ F ₄ ↔ ³ H ₆	4.37	0.5688	0.6130	0.4616	0
³ F ₄ ↔ ³ H ₅	2.25	0.0295	0.3129	0.4399	0.167
³ F ₄ ↔ ³ H ₄	1.53	0.0193	0.0505	0.4917	0.171
¹ G ₄ ↔ ³ F ₄	3.42	0.0789	0.1445	0.3490	2.689
¹ G ₄ ↔ ³ F ₃	2.96	0.0039	0.0055	0.0524	2.377
¹ G ₄ ↔ ³ F ₂	2.10	0.0000	0.0161	0.0063	0
¹ G ₄ ↔ ³ H ₆	1.92	0.2568	0.2568	0.2432	0
¹ G ₄ ↔ ³ H ₅	1.36	0.0380	0.0985	0.4205	0.147
¹ G ₄ ↔ ³ H ₄	1.06	0.0014	0.0065	0.0230	0.060
¹ D ₂ ↔ ¹ G ₄	1.43	0.2956	0.0518	0.0755	0
¹ D ₂ ↔ ³ F ₄	1.01	0.6051	0.0000	0.0200	0
¹ D ₂ ↔ ³ F ₃	0.96	0.0327	0.0185	0	0.148
¹ D ₂ ↔ ³ F ₂	0.85	0.0140	0.0872	0	0.078
¹ D ₂ ↔ ³ H ₆	0.82	0	0.0707	0.0061	0
¹ D ₂ ↔ ³ H ₅	0.70	0	0.0023	0.0003	0
¹ D ₂ ↔ ³ H ₄	0.61	0.0031	0.0172	0.0541	0
³ P ₀ ↔ ¹ D ₂	2.73	0.0154	0	0	0
³ P ₀ ↔ ¹ G ₄	0.94	0	0.0558	0	0
³ P ₀ ↔ ³ F ₄	0.74	0	0.1067	0	0
³ P ₀ ↔ ³ F ₃	0.71	0	0	0	0
³ P ₀ ↔ ³ F ₂	0.65	0.2951	0	0	0
³ P ₀ ↔ ³ H ₆	0.63	0	0	0.0727	0
³ P ₀ ↔ ³ H ₅	0.55	0	0	0	0
³ P ₀ ↔ ³ H ₄	0.50	0	0.1729	0	0
¹ I ₆ ↔ ³ P ₀	869	0	0	0.0031	0
¹ I ₆ ↔ ¹ D ₂	2.72	0	0.1554	1.7042	0
¹ I ₆ ↔ ¹ G ₄	0.94	0.2426	1.3860	0.6684	0

3.4. Luminescence spectra

In order to characterize the Pr:Lu₂S₃ luminescence spectra in detail, and to assign the observed spectral lines to the corresponding transitions, several excitation wavelengths were employed to selectively excite the main energy levels (namely ³P₂, ¹D₂, ¹G₄, and ³F₄) of the Pr:Lu₂S₃ material. All measurements were carried out at room temperature. In total, the obtained luminescence spectra of the Pr:Lu₂S₃ crystal covered the wavelength range from 460 nm to 5.4 μm.

3.4.1. Excitation of ³P₂ energy level

The ³P₂ level was excited by radiation with a wavelength of 456 nm. During this excitation, no emission at a wavelength below 497 nm was observed, as shown in the luminescence spectra in Fig. 6. Taking into account the proximity of the ³P₂, ³P₁ and ³P₀ levels, the majority of the Pr³⁺ ions are expected to relax rapidly to the ³P₀ or ¹I₆ state. Furthermore, considering the size of the squared reduced-matrix elements for the tensor operators $U^{(k)}$, it can be assumed that most of the observed emission lines correspond to transitions originating from the ³P₀ level. However, to explain the origin of some emission lines, it was necessary to acknowledge that the starting level is also ¹I₆ (transitions ¹I₆ → ³H₅, ¹I₆ → ³F₃, ¹I₆ → ¹G₄), since the corresponding transitions starting from the ³P₀ level are either forbidden or very unlikely, see Tab. 2 (from this point of view it is noteworthy that although the values of $|\langle U^{(2,4,6)} \rangle|^2$ for ¹I₆ → ¹G₄ transition belongs to the largest, the corresponding emission is rather less intense).

It should be noted that upon excitation of the ³P₂ level, spectral lines

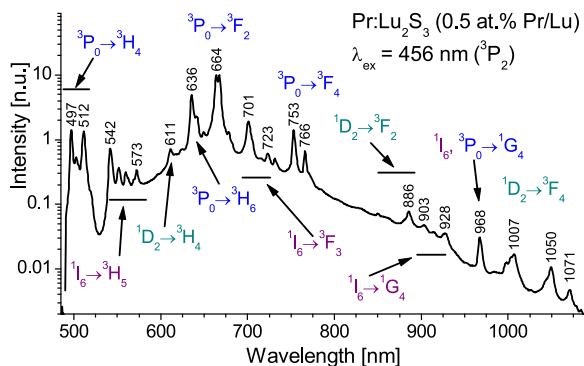


Fig. 6. Luminescence spectra of Pr:Lu₂S₃ corresponding to ³P₂ excitation at wavelength 456 nm measured by BlueWave spectrometer in range 480 – 1080 nm. Transitions with a different starting energy level are distinguished by a different color.

associated with ¹D₂ level transitions are also observable in the emission spectrum, see Fig. 6. This is evident by comparison of that spectrum with the spectrum obtained upon direct excitation of the ¹D₂ level, as described in 3.4.2 (Fig. 7).

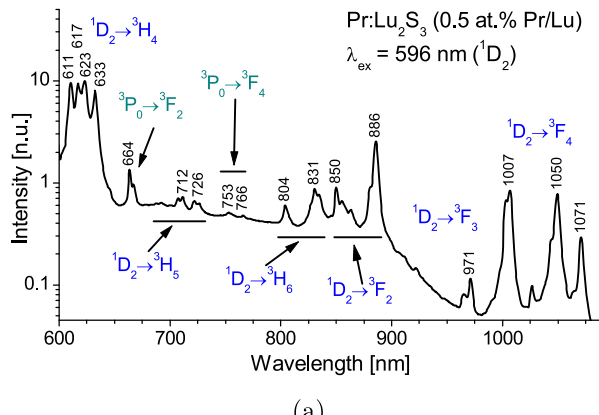
It is also worth mentioning, the luminescence spectra (see Fig. 6 and Fig. 7a) are distorted by the luminescence signal originating from the color centers in the crystal which are characterized by the broad emission, typically in the visible spectral range, resulting in a pedestal-like background in the measured spectra. The precise nature of the color center has not yet been investigated. However, sulfur vacancies and the substitution of sulfur by oxygen are considered the most likely origins.

3.4.2. Excitation of ¹D₂ energy level

The luminescence spectra obtained upon excitation of the ¹D₂ level by the 596 nm wavelength radiation are depicted in Fig. 7, along with the respective transitions. Besides the expected spectral lines originating from the ¹D₂ level, followed by the transitions from the subsequent lower energy levels (¹G₄, ³F₄, and ³F₃), there are some lines in the spectrum (namely 664, 753, and 766 nm) which can not be assigned to any of these transitions (based on the calculated squared reduced-matrix elements for the tensor operators U^(k), see Tab. 2). Nevertheless, these lines can be well explained by transitions from the ³P₀ level. Therefore, the hypothesis is that there exists some energy transfer processes, such as the absorption of excited states (e.g. ³H₆ → ³P₁ or ³F₃ → ³P₂), which populate the ³P₀ level.

3.4.3. Excitation of ¹G₄ energy level

In the case of the ¹G₄ level excitation, radiation at 1022 nm



(a)

wavelength was used. The corresponding luminescence spectra recorded in the range of 1200 – 1700 nm, 1750 – 2040 nm, and 2000 – 3600 nm are shown in Fig. 8a, b, and Fig. 8c, respectively.

Note, the spectrum assigned to the ¹G₄ → ³H₅ transition exactly matches the corresponding part of the spectrum observed upon excitation of the ¹D₂ level (see Fig. 7b). If we assume that the sensitivity of the dedicated spectrometer does not vary significantly within the specified measuring spectral range, it can be reasonably deduced (from Fig. 7b) that the majority (approx. 75 %) of Pr³⁺ ions excited to the level ¹G₄ will subsequently leave this level directly via the channel ¹G₄ → ³H₅. This deduction is based on the ratio of the integrated parts of the luminescence spectrum shown in Fig. 7b, which are associated with the transitions ¹G₄ → ³H₅ and ¹D₂ → ¹G₄. From the data presented in Fig. 8a, we know the exact spectrum corresponding to the pure ¹G₄ → ³H₅ transition. The integral over this spectrum, covering the 1270 – 1410 nm range, is 25.5 au · nm, and this value is proportional to the number of ¹G₄ → ³H₅ transitions. We expect that the luminescence within the 1410 – 1610 nm spectral range (see Fig. 7b) corresponds to the ¹D₂ → ¹G₄ transition, with the respective integral of 34 au · nm. This value is proportional to the number of ¹D₂ → ¹G₄ transitions. The ratio of these integrals is 0.75, meaning that 75 % of the photons reaching the ¹G₄ level via the ¹D₂ → ¹G₄ transition leave this level through the ¹G₄ → ³H₅ channel.

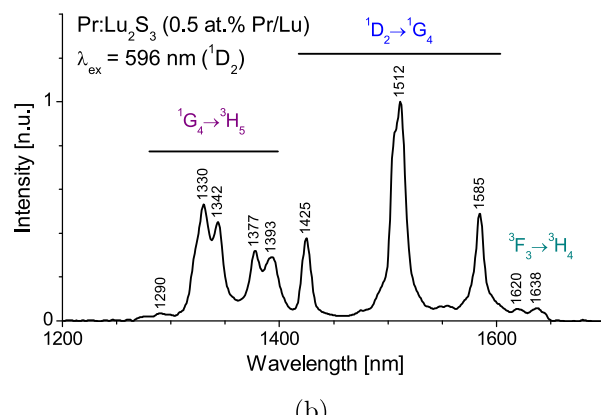
Furthermore, luminescence around a wavelengths of 1.9 μm, 3 μm, and 3.4 μm which can be assigned to the ¹G₄ → ³H₆, ¹G₄ → ³F₃ and ¹G₄ → ³F₄ transitions, respectively, was observed. It should be remarked that the recorded spectrum corresponding to ¹G₄ → ³F₄ transition was constrained by the range of the Pbs detector used. Therefore, it is possible that this emission may extend further into the infrared region.

3.4.4. Excitation of ³F₄ energy level

The Pr:Lu₂S₃ emission recorded upon excitation of the ³F₄ and ³F₃ levels is also of great interest, because it covers wide spectral bands in the infrared region with the potential to generate radiation of up to ~7 μm wavelength. A large number of sublevels corresponding to ³F₄ and ³F₃ levels provide a series of relatively broad absorption bands from 1.4 to 1.7 μm (see Fig. 5b), which can be easily excited by many commercially available pumping sources, like laser diodes, Er-doped fiber or Raman fiber lasers.

The luminescence spectra obtained upon excitation of the ³F₄ level by 1453 nm wavelength radiation are displayed in Fig. 9, for the spectral range of the 1500 nm – 1700 nm (³F_{4,3} → ³H₄ transition).

Subsequently, radiation with a wavelength of 1556 nm was used to excite the ³F_{4,3} level, which provided a more intense luminescence signal. With the help of a monochromator along with the sensitive detectors, the emission spectra in the range of 1.9 – 2.8 μm (Fig. 10a) and 4 – 5.4 μm (Fig. 10b) were obtained. It should be remarked, that the



(b)

Fig. 7. Luminescence spectra of Pr:Lu₂S₃ corresponding to ¹D₂ excitation at wavelength 596 nm measured by BlueWave spectrometer in range 600 – 1080 nm (a) and by DwarfStar spectrometer in range 1200 – 1700 nm (b). Transitions with a different starting energy level are distinguished by a different color.

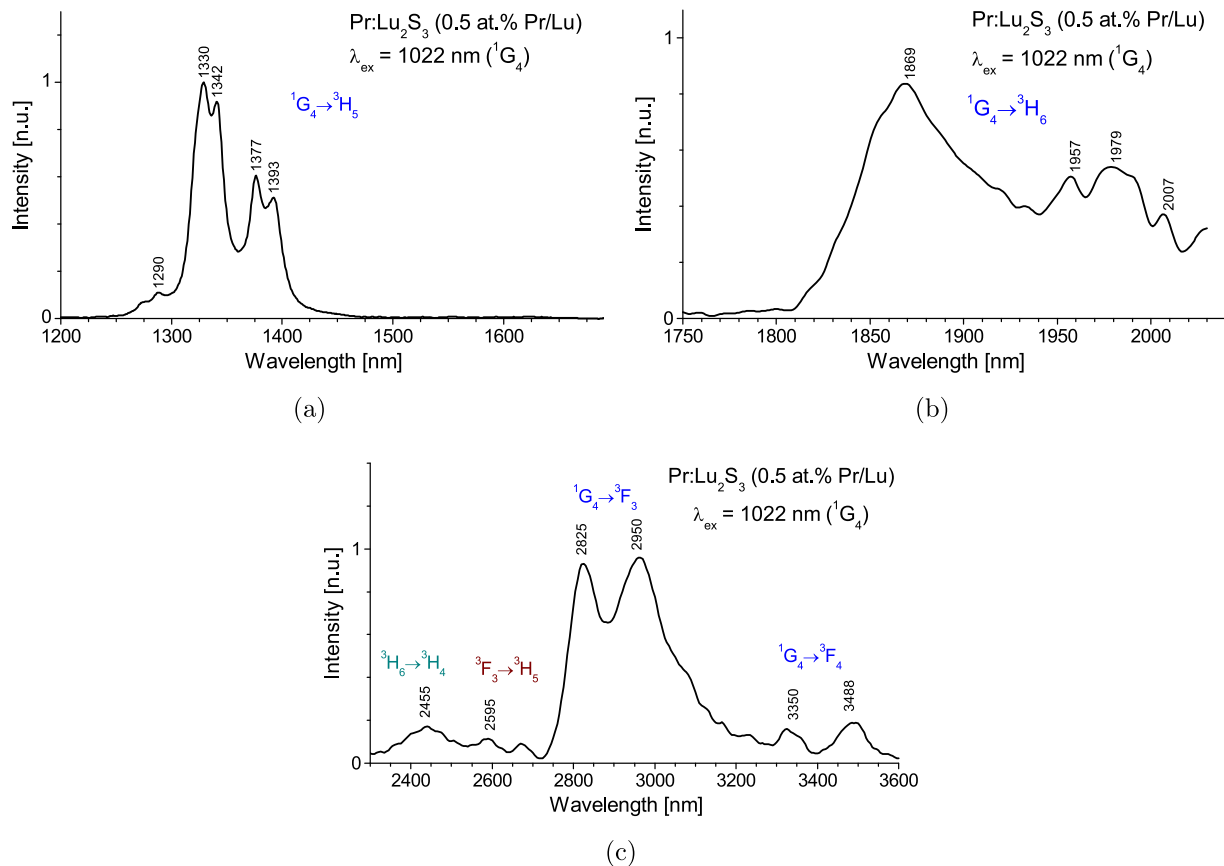


Fig. 8. Luminescence spectra of Pr:Lu₂S₃ corresponding to ¹G₄ excitation at wavelength 1022 nm measured behind the 1.2 μ m long-pass filter (FELH1200, Thorlabs) by DwarfStar spectrometer in range 1.2 – 1.7 μ m (a), by Oriel monochromator (slit width 1.3 mm) in combination with PbS detector and long-pass filter (FEL 1500, Thorlabs) in range 1.75 – 2.04 μ m (b), and by Oriel monochromator (slit width 2 mm) along with PbS detector and 2.05 μ m long-pass filter (LP-2050, Spectrogon) in range 2.3 – 3.6 μ m (c). Transitions with a different starting energy level are distinguished by a different color.

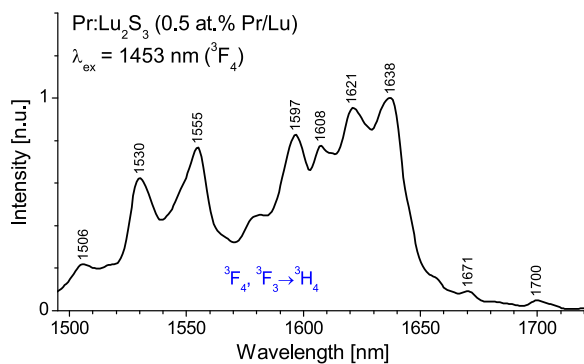


Fig. 9. Luminescence spectra of Pr:Lu₂S₃ corresponding to ³F₄ excitation at wavelength 1453 nm and subsequent transition ³F_{4,3} \rightarrow ³H₄ measured by DwarfStar spectrometer in range 1500 – 1700 nm behind the 1.5 μ m long-pass filter (FELH1500, Thorlabs).

part of the spectrum above 5 μ m (Fig. 10b) is affected by the decreasing sensitivity of the PbSe detector.

Moreover, it can be reasonably assumed that upon excitation of the ³F_{4,3} level, luminescence transitions even at ³F₃ \rightarrow ³H₆ (\sim 5.5 μ m) and ³F₃ \rightarrow ³F₂ (\sim 7 μ m) can be reached from the Pr:Lu₂S₃ material. This assumption is based on the following deduction: the distance between the ³F₂ and ³F₃ level barycenters (described in subsection 3.3) is only \sim 1400 cm^{-1} (see Tab. 1), so the gap between the lowest ³F₃ sublevel and the highest ³F₂ sublevel will be even smaller, thus only 4 phonons may be enough to overcome it (given the estimated phonon energy of 312

cm⁻¹ for Lu₂S₃). For that reason, one could expect significant non-radiative depopulation of the ³F₃ level. However, the observed luminescence from this level is proof that ³F₃ is only weakly quenched by multiphonon relaxation in the case of Pr:Lu₂S₃. Therefore, it is legitimate to expect that with appropriate detector it would be possible to observe emission even at wavelengths of up to 7 μ m.

4. Conclusion

Spectroscopic properties of a new low-phonon material, Pr:Lu₂S₃, prepared by a modified micro-pulling-down method, were presented. The Pr:Lu₂S₃ was investigated for its potential application as a low-phonon solid state laser material for mid-IR laser sources; excitation and luminescence spectra up to 5.4 μ m were described, for the first time to our best knowledge. To characterize the luminescence spectra of the Pr:Lu₂S₃ in detail, several excitation wavelengths were used to excite the main energy levels of the Pr³⁺-ion; doing that along with the help of the calculated squared reduced-matrix elements, 26 transitions associated to the measured emission spectra were identified in the energy level structure of the Pr:Lu₂S₃.

In addition, calculated barycenters, intermediate coupling wavefunctions, and optimized squared reduced-matrix elements for tensor operators $U^{(k)}$ and $L + gS$ are presented in this contribution for the Pr:Lu₂S₃ material. Our next goal is to use these values for the Judd-Ofelt analysis in the future, to obtain even more information about this crystal, providing, the quality of the grown sample will be enough to determine the Pr:Lu₂S₃ absorption cross-sections.

It should be noted that the poor quality of the grown sample, which is limited by the current material preparation technology, prevents the

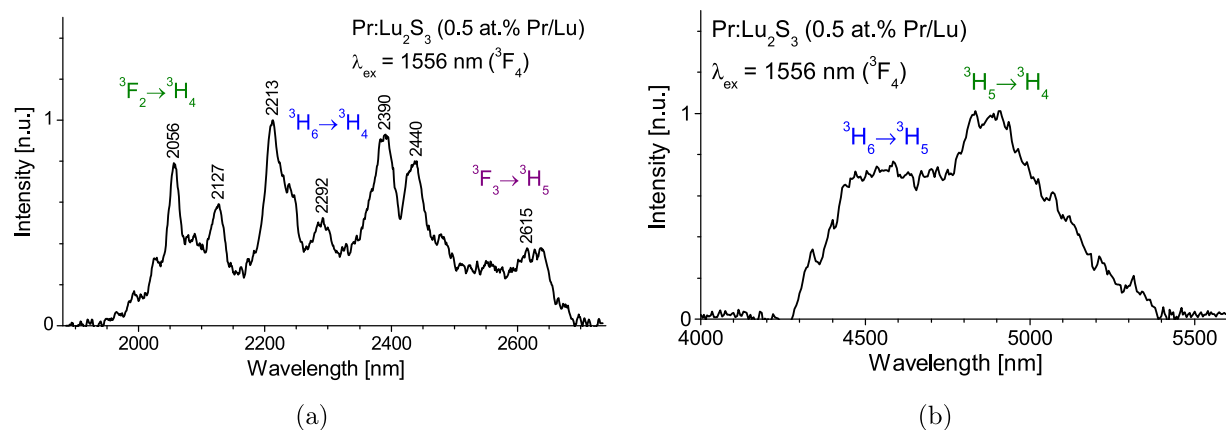


Fig. 10. Luminescence spectra of Pr:Lu₂S₃ for the spectral range of 1.9 – 2.8 μm (monochromator Oriel, slit width 1 mm, PbS detector and long-pass filter LP-1850, Spectrogon) (a) and 4 – 5.5 μm (monochromator Oriel, slit width 8 mm, PbSe detector and long-pass filter LP-3000, Spectrogon) (b). Transitions with a different starting energy level are distinguished by a different color.

acquisition of relevant data necessary to determine the fluorescence lifetime. Defects and color centers in the crystal may act as trapping centers or contribute to quenching mechanisms, leading to potentially misleading results. Once improvements are made in the growth technology (e.g., by selecting a more appropriate crucible, as described in 2.1) and higher-quality samples become available, we plan to build on the existing knowledge and fully spectroscopically characterize the crystal.

It should be also remarked that although we cannot directly compare (as explained earlier in the text) Lu₂S₃ properties such as lifetimes, effective cross-sections, and/or multi-phonon relaxation rates with those of other well-established low-phonon laser hosts, we believe the host matrix itself has no direct competitor among the low-phonon materials. We are not aware of any matrices that are simultaneously comparable to Lu₂S₃ in all key parameters, such as being low-phonon, transparent in the deep infrared region, non-hygroscopic, and tolerant to high doping concentrations of lanthanide ions. In this regard, the Lu₂S₃ is unique. The only comparable material is the KLuS₂ crystal, but it has not yet been successfully grown in bulk form.

So, based on the presented results, it can be concluded that Pr:Lu₂S₃ material has the potential to be an interesting candidate for mid-infrared laser sources. In addition, the Lu₂S₃ matrix is definitely attractive for further lanthanide doping.

CRediT authorship contribution statement

Martin Fibrich: Writing – original draft, Visualization, Methodology, Investigation, Formal analysis, Data curation, Conceptualization. **Lubomír Havlák:** Writing – review & editing, Validation, Methodology, Investigation, Conceptualization. **Jan Šulc:** Writing – review & editing, Visualization, Validation, Methodology, Investigation, Formal analysis, Data curation, Conceptualization. **Robert Král:** Writing – review & editing, Validation, Methodology, Investigation, Conceptualization. **Vítězslav Jarý:** Writing – review & editing, Validation, Methodology, Conceptualization. **David Vyhlídal:** Writing – review & editing, Visualization, Software. **Vojtěch Vaněček:** Writing – review & editing, Methodology, Investigation, Conceptualization. **Martin Nikl:** Writing – review & editing, Supervision, Resources, Funding acquisition. **Helena Jelínková:** Writing – review & editing, Supervision, Resources, Project administration, Funding acquisition, Conceptualization.

Funding

The work is supported by Operational Programme Johannes Amos Comenius financed by European Structural and Investment Funds and

the Czech Ministry of Education, Youth and Sports (Project LASCIMAT – CZ.02.01.01/00/23_020/0008525).

Declaration of Competing Interest

The authors declare that they have no known competing financial interests or personal relationships that could have appeared to influence the work reported in this paper.

References

- [1] M. Velázquez, A. Ferrier, J.-L. Doualan, R. Moncorgé, Rare-earth-doped low phonon energy halide crystals for mid-infrared laser sources, in: A.H. Al-Khursan (Ed.), Solid State Laser, IntechOpen, Rijeka, 2012, <https://doi.org/10.5772/38204>.
- [2] J.-L. Doualan, R. Moncorgé, Laser crystals with low phonon frequencies, Ann. De. Chim. Sci. Des. Mater. Ann Chim Sci Mater. 28 (2003) 5–20, <https://doi.org/10.1016/j.annchem.2003.09.004>.
- [3] L. Isaenko, A. Yelisseyev, A. Tkachuk, S. Ivanova, New monocrystals with low phonon energy for mid-IR lasers, in: M. Ebrahim-Zadeh, I.T. Sorokina (Eds.), Mid-Infrared Coherent Sources and Applications, Springer, Netherlands, Dordrecht, 2008, pp. 3–65.
- [4] S.R. Bowman, L.B. Shaw, B.J. Feldman, J. Ganem, A 7 μ m praseodymium-based solid-state laser, IEEE J. Quantum Electron. 32 (1996) 646–649. (<https://api.semanticscholar.org/CorpusID:117012748>).
- [5] A. Garcia-Adreva, R. Balda, J. Fernandez, Laser cooling of Er³⁺-doped low-phonon materials: current status and outlook, Opt. Mater. 31 (2009) 1075–1081, <https://doi.org/10.1016/j.optmat.2008.01.020>.
- [6] S.M. Kirkpatrick, L.B. Shaw, S.R. Bowman, S. Searles, B.J. Feldman, J. Ganem, Mid-infrared spectroscopy of erbium doped chloride laser crystals, Opt. Express 1 (4) (1997) 78–86, <https://doi.org/10.1364/OE.1.000078>. (<https://optg.optica.org/oe/abstract.cfm?URI=oe-1-4-78>).
- [7] K. Nitsch, M. Dušek, M. Nikl, K. Polák, M. Rodová, Ternary alkali lead chlorides: crystal growth, crystal structure, absorption and emission properties, Prog. Cryst. Growth Charact. Mater. 30 (1) (1995) 1–22, [https://doi.org/10.1016/0960-8974\(95\)00012-V](https://doi.org/10.1016/0960-8974(95)00012-V).
- [8] K. Rademaker, Rare Earth-Doped Alkali-Lead-Halide Laser Crystals of Low-Phonon Energy, Cuvillier Verlag, Göttingen, 2005.
- [9] M. Fibrich, J. Šulc, R. Král, V. Jarý, M. Němec, H. Jelínková, A. Bystrický, P. Zemenová, M. Nikl, Luminescence study of rare-earth (RE)-doped low-energy phonon RbPb₂Cl₅ crystals for mid-infrared (IR) lasers emitting above 4.5 μ m wavelength, Laser Phys. 29 (7) (2019) 075801, <https://doi.org/10.1088/1555-6611/ab1481>.
- [10] S. Payne, M. Nostrand, R. Page, P. Schunemann, L. Isaenko, Laser demonstration of rare-earth ions in low phonon chloride and sulfide crystals, in: Proceedings of the ASSL, OSA, 2000, MF4.10.1364/ASSL.2000.MF4.
- [11] S.R. Bowman, S.K. Searles, N.W. Jenkins, S.B. Qadri, E.F. Skelton, J. Ganem, New mid-IR laser based on an erbium activated low phonon energy crystal, In: Proceedings of the Technical Digest, Summaries of Papers Presented at the Conference on Lasers and Electro-Optics, Postconference Technical Digest, IEEE Cat. No.01CH37170, 2001, 557–558.10.1109/CLEO.2001.948162.
- [12] L. Isaenko, A. Yelisseyev, A. Tkachuk, S. Ivanova, S. Vatnik, A. Merkulov, S. Payne, R. Page, M. Nostrand, New laser crystals based on Kpb₂Cl₅ for IR region, Mater. Sci. Eng. B 81 (1) (2001) 188–190, [https://doi.org/10.1016/S0921-5107\(00\)00735-2](https://doi.org/10.1016/S0921-5107(00)00735-2).
- [13] A.G. Okhrimchuk, L.N. Butvina, E.M. Dianov, N.V. Lichkova, V.N. Zagorodnev, A. V. Shestakov, New laser transition in a Pr³⁺:RbPb₂Cl₅ crystal in the 2.3–2.5-μ m

range, *Quantum Electron.* 36 (1) (2006) 41, <https://doi.org/10.1070/QE2006v03n01ABEH013101>.

[14] A.G. Okhrimchuk, L.N. Butvina, E.M. Dianov, I.A. Shestakova, N.V. Lichkova, V. N. Zagorodnev, A.V. Shestakov, Optical spectroscopy of the $\text{RbPb}_2\text{Cl}_5\text{Dy}^{3+}$ laser crystal and oscillation at $5.5 \mu\text{m}$ at room temperature, *J. Opt. Soc. Am. B Opt. Phys.* 24 (10) (2007) 2690–2695, <https://doi.org/10.1364/JOSAB.24.002690>.

[15] L.D. DeLoach, R.H. Page, G.D. Wilke, S.A. Payne, W.F. Krupke, Transition metal-doped zinc chalcogenides: spectroscopy and laser demonstration of a new class of gain media, *IEEE J. Quantum Electron.* 32 (6) (1996) 885–895, <https://doi.org/10.1109/3.502365>.

[16] R. Page, K. Schaffers, L. DeLoach, G. Wilke, F. Patel, J. Tassano, S. Payne, W. Krupke, K.-T. Chen, A. Burger, Cr^{2+} -doped zinc chalcogenides as efficient, widely tunable mid-infrared lasers, *IEEE J. Quantum Electron.* 33 (4) (1997) 609–619, <https://doi.org/10.1109/3.563390>.

[17] T.J. Carrig, Transition-metal-doped chalcogenide lasers, *J. Electron. Mater.* 31 (7) (2002) 759–769, <https://doi.org/10.1007/s11664-002-0233-1>.

[18] V.A. Akimov, A.A. Voronov, V.I. Kozlovskii, Y.V. Korostelin, A.I. Landman, Y. P. Podmar'kov, M.P. Frolov, Efficient IR Fe:ZnSe laser continuously tunable in the spectral range from 3.77 to 4.40 μm , *Quantum Electron.* 34 (10) (2004) 912, <https://doi.org/10.1070/QE2004v03n10ABEH002789>.

[19] V. Fedorov, S. Mirov, A. Gallian, D. Badikov, M. Frolov, Y. Korostelin, V. Kozlovsky, A. Landman, Y. Podmar'kov, V. Akimov, A. Voronov, 3.77–5.05- μm tunable solid-state lasers based on Fe^{2+} -doped ZnSe crystals operating at low and room temperatures, *IEEE J. Quantum Electron.* 42 (9) (2006) 907–917, <https://doi.org/10.1109/JQE.2006.880119>.

[20] M.E. Doroshenko, H. Jelínková, P. Koranda, J. Šulc, T.T. Basiev, V.V. Osiko, V. K. Komar, A.S. Gerasimenko, V.M. Puzikov, V.V. Badikov, D.V. Badikov, Tunable mid-infrared laser properties of $\text{Cr}^{2+}\text{ZnMgSe}$ and $\text{Fe}^{2+}\text{ZnSe}$ crystals, *Laser Phys. Lett.* 7 (1) (2010) 38–45, <https://doi.org/10.1002/lapl.200910111>.

[21] M.E. Doroshenko, V.V. Osiko, H. Jelínková, M. Jelínek, J. Šulc, D. Vyhlídal, N. O. Kovalenko, I.S. Terzin, Spectral and lasing characteristics of $\text{Fe:Cd}_{1-x}\text{Mn}_x\text{Te}$ ($x = 0.1 - 0.76$) crystals in the temperature range 77 to 300 K, *Opt. Mater. Express* 8 (7) (2018) 1708–1722, <https://doi.org/10.1364/OME.8.001708>.

[22] T.T. Basiev, M.E. Doroshenko, V.V. Osiko, D.V. Badikov, Mid IR laser oscillations in new low phonon $\text{PbGa}_2\text{S}_4\text{Dy}^{3+}$ crystal, in: C. Denman, I. Sorokina (Eds.), ASSL (TOPS), Vol. 98 of OSA Trends in Optics and Photonics, OSA, 2005, p. 75, <https://doi.org/10.1364/ASSP.2005.75>.

[23] M.E. Doroshenko, T.T. Basiev, V.V. Osiko, V.V. Badikov, D.V. Badikov, H. Jelínková, P. Koranda, J. Šulc, Oscillation properties of dysprosium-doped lead thiogallate crystal, *Opt. Lett.* 34 (5) (2009) 590–592, <https://doi.org/10.1364/OL.34.000590>.

[24] H. Jelínková, M.E. Doroshenko, M. Jelínek, J. Šulc, V.V. Osiko, V.V. Badikov, D. V. Badikov, Dysprosium-doped PbGa_2S_4 laser generating at 4.3 μm directly pumped by 1.7 μm laser diode, *Opt. Lett.* 38 (16) (2013) 3040–3043, <https://doi.org/10.1364/OL.38.003040>.

[25] L. Havlák, V. Jarý, M. Nikl, P. Boháček, J. Bárta, Preparation, luminescence and structural properties of RE-doped RbLa_2O_3 compounds, *Acta Mater.* 59 (16) (2011) 6219–6227, <https://doi.org/10.1016/j.actamat.2011.06.019>.

[26] V. Jarý, L. Havlák, J. Bárta, M. Nikl, Preparation, luminescence and structural properties of rare-earth-doped RbLu_2O_3 compounds, *Phys. Status Solidi RRL* 6 (2) (2012) 95–97, <https://doi.org/10.1002/pssr.201105481>.

[27] V. Jarý, L. Havlák, J. Bárta, E. Mihóková, M. Buryi, M. Nikl, $\text{AlLn}_2\text{S}_2\text{RE}$ ($\text{A} = \text{K, Rb; L} = \text{La, Gd, Lu, Y}$): new optical materials family, *J. Lumin.* 170 (2016) 718–735, <https://doi.org/10.1016/j.jlumin.2015.08.080>.

[28] J. Šulc, R. Švejkar, M. Fibrich, H. Jelínková, L. Havlák, V. Jarý, M. Ledinský, M. Nikl, J. Bárta, M. Buryi, R. Lorenzi, F. Cova, A. Vedda, Infrared spectroscopic properties of low-phonon lanthanide-doped KLu_2S_2 crystals, *J. Lumin.* 211 (2019) 100–107, <https://doi.org/10.1016/j.jlumin.2019.03.005>. (<https://www.sciencedirect.com/science/article/pii/S0022231319300699>).

[29] V. Sokolov, A. Kamarzin, L. Trushnikova, M. Savelyeva, Optical materials containing rare earth Ln_2S_3 sulfides, in: Proceedings of the Second International Conference on f-Elements, *J. Alloy. Compd.* 225 (1) (1995) 567–570, [https://doi.org/10.1016/0925-8388\(94\)07063-6](https://doi.org/10.1016/0925-8388(94)07063-6). (<https://www.sciencedirect.com/science/article/pii/0925838894070636>).

[30] C.M. Forster, W.B. White, Optical absorption edge in rare earth sesquisulfides, *Mater. Res. Bull.* 41 (2) (2006) 448–454, <https://doi.org/10.1016/j.materresbull.2005.07.035>. (<https://www.sciencedirect.com/science/article/pii/S0025540805002977>).

[31] X. Zhang, W. Gui, Q. Wu, Q. Zeng, Structural, phonon, mechanical, optical, and thermodynamic properties of stable $\beta\text{-La}_2\text{S}_3$ from first-principles calculations, *J. Rare Earths* 35 (3) (2017) 271–279, [https://doi.org/10.1016/S1002-0721\(17\)60910-4](https://doi.org/10.1016/S1002-0721(17)60910-4). (<https://www.sciencedirect.com/science/article/pii/S1002072117609104>).

[32] J. Gruber, B. Zandi, B. Justice, E. Westrum Jr, Optical spectra and thermal schottky levels in the high temperature γ -phase of the lanthanide sesquisulfides, *J. Phys. Chem. Solids* 61 (8) (2000) 1189–1197, [https://doi.org/10.1016/S0022-3697\(99\)00417-5](https://doi.org/10.1016/S0022-3697(99)00417-5). (<https://www.sciencedirect.com/science/article/pii/S0022369799004175>).

[33] W. Xu, G. Bai, E. Pan, D. Li, J. Zhang, S. Xu, Advances, optical and electronic applications of functional materials based on rare earth sulfide semiconductors, *Mater. Des.* 238 (2024) 112698, <https://doi.org/10.1016/j.matdes.2024.112698>. (<https://www.sciencedirect.com/science/article/pii/S0264127524000704>).

[34] A. Kamarzin, K. Mironov, V. Sokolov, Y. Malovitsky, I. Vasil'yeva, Growth and properties of lanthanum and rare-earth metal sesquisulfide crystals, *J. Cryst. Growth* 52 (1981) 619–622, [https://doi.org/10.1016/0022-0248\(81\)90351-1](https://doi.org/10.1016/0022-0248(81)90351-1). (<https://www.sciencedirect.com/science/article/pii/0022024881903511>).

[35] M. Kanazawa, L. Li, T. Kuzuya, K. Takeda, S. Hirai, Y. Higo, T. Shimpei, T. Irifune, C. Sekine, High-pressure and high-temperature synthesis of heavy lanthanide sesquisulfides Ln_2S_3 ($\text{Ln} = \text{Yb}$ and Lu), *J. Alloy. Compd.* 736 (2018) 314–321, <https://doi.org/10.1016/j.jallcom.2017.11.090>. (<https://www.sciencedirect.com/science/article/pii/S0925838817338367>).

[36] V. Vaněček, V. Jarý, R. Král, L. Havlák, A. Vlk, R. Kučerková, J.B. Průša, M. Nikl, Growth and spectroscopic properties of Pr^{3+} doped Lu_2S_3 single crystals, *Cryst. Growth Des.* 24 (11) (2024) 4736–4742, <https://doi.org/10.1021/acs.cgd.4c00330>.

[37] M. Fibrich, J. Šulc, R. Švejkar, H. Jelínková, Continuous-wave efficient cyan-blue Pr:YAlO_3 laser pumped by InGaN laser diode, *Appl. Phys. B* 127 (2) (2020) 1–6, <https://doi.org/10.1007/s00340-020-07546-w>.

[38] H. Ogino, A. Yoshikawa, M. Nikl, K. Kamada, T. Fukuda, Scintillation characteristics of Pr-doped $\text{Lu}_3\text{Al}_5\text{O}_12$ single crystals, *J. Cryst. Growth* 292 (2) (2006) 239–242, <https://doi.org/10.1016/j.jcrysgr.2006.04.021>.

[39] M. Sugiyama, Y. Yokota, Y. Fujimoto, T. Yanagida, Y. Futami, S. Kurosawa, A. Yoshikawa, Dopant segregation in rare earth doped lutetium aluminum garnet single crystals grown by the micro-pulling down method, *J. Cryst. Growth* 352 (1) (2012) 110–114, <https://doi.org/10.1016/j.jcrysgr.2011.12.039>.

[40] M.P. Hehlen, M.G. Brik, K.W. Kramer, 50th anniversary of the Judd-Oelft theory: an experimentalist's view of the formalism and its application (pdf), *J. Lumin.* 136 (2013) 221–239, <https://doi.org/10.1016/j.jlumin.2012.10.035>. (<http://www.sciencedirect.com/science/article/pii/S0022231312006217>) (pdf).

[41] M.P. Hehlen, RELIC 1.0 – Rare Earth Level and Intensity Calculations(2013). (<https://www.lanl.gov/projects/feynman-center/deploying-innovation/intellectual-property/software-tools/relic/>).

[42] A.A. Kaminskii, Crystalline lasers: physical processes and operating schemes. *Laser Science & Technology Series*, CRP Pres, Inc, Florida, USA, 1996, <https://doi.org/10.1604/9780849337208> (<https://www.crcpress.com/Crystalline-Lasers-Physical-Processes-and-Operating-Schemes/Kaminskii/p/book/9780849337208>).